

In-plane optical features of the underdoped and optimally doped $\text{La}_{2-x}\text{Sr}_x\text{CuO}_4$ compounds: Theoretical multiband analysis

Ivan Kupčić

Department of Physics, Faculty of Science, POB 331, HR-10 002 Zagreb, Croatia

Three-component *ab*-plane optical conductivity of the high- T_c cuprates is developed by using the gauge invariant transverse response theory, and compared to the spectral functions previously obtained from the optical reflectivity measurements in $\text{La}_{2-x}\text{Sr}_x\text{CuO}_4$, $x < 0.2$. The conducting electrons are described by the Emery three-band model with the short-range correlations modeled by an effective (quasi)dimerization potential and (for $\delta < 0.1$) by a doping-dependent bond-energy renormalization parameter. In the $0.1 < \delta < 0.2$ doping range, it is shown that the total spectral weight of the three-band model is shared between the intraband and interband channels nearly in equal proportions. The corresponding intraband conductivity has a (non-Drude) nearly single-component form, which transforms with decreasing doping into a two-component structure at $\delta < 0.1$. The calculated interband conductivity is characterized by a well-distinguished pick, and agrees well with the measured spectra in the $x < 0.1$ compounds. The gauge invariant form of the static and elastic Raman vertices is determined, allowing explicit verification of the effective mass theorem and the related conductivity sum rules. The intimate connection between the present three-component model and the experimental spectra is established by using relatively large damping energies, at variance with similar multi-oscillator (i.e. multi-parameter) optical models characterized by small damping effects. In particular, the anomalous hardening of the mid-infrared pick with decreasing doping seems to be a result of an additional increase in the related damping energy.

PACS numbers: 74.25.Gz 74.25.Nf

Keywords: superconductivity, high- T_c cuprates, $\text{La}_{2-x}\text{Sr}_x\text{CuO}_4$, optical properties, conductivity sum rules, Raman vertex functions

I. INTRODUCTION

Systematic optical and Raman-scattering studies of the high- T_c cuprates[1, 2, 3, 4] have renewed the theoretical interest for the interband optical processes in the metallic compounds, giving preference to the optical theories based on the multiband models[5, 6, 7]. The optical analyses of the metallic cuprates are usually limited on the low-frequency spectra (typically, $\hbar\omega < 1.5$ eV), and use different single-band models[8, 9, 10, 11]. Similarly, the related Raman-scattering analyses[12, 13, 14, 15, 16] employ the analogous static-Raman-vertex approximation. Several anomalies observed in the doping- and temperature-dependence measurements cannot be quantitatively explained by such single-band approaches. The most interesting anomalies of this kind are the following. (i) The softening and narrowing of the mid-infrared pick with increasing doping[1, 2], or with decreasing temperature[4]. (ii) Surprisingly rapid loss of the spectral weight below the charge-transfer gap with decreasing doping, for $\delta < 0.1$.[1, 2] (iii) The resonant behavior of both the interband conductivity and the “two-magnon” Raman-scattering contribution at $\delta < 0.1$ for the photon energies near the charge-transfer energy.[2]

In this paper, we consider the response of the conducting electrons described by the Emery three-band model[17] on the external vector potential, and develop the three-component optical conductivity comprised of the Drude, mid-infrared, and interband contributions. By comparing the model predictions with the experimental data, we can estimate the values of the model

parameters. The reconciliation of the spectra obtained from the optical reflectivity measurements (the real part of the optical conductivity, the corresponding integrated spectral weight, and the real part of the dielectric function) with the present optical model, or with some other experimental probes, can be tested in this way.

Section II A, together with the Appendices, describes an exactly solvable version of the model obtained by disregarding the correlation effects. By using this model, we prove the gauge invariance of the present response theory, and determine the gauge invariant form of the static and elastic Raman vertices.

In Sec. II B, the effect of the spin-density (or charge-density) fluctuations of the wave vector $(\pi/a, \pi/a)$ on the low-frequency optical conductivity is described within the adiabatic approximation, leading to the (quasi)dimerization of the conducting band with a strong influence on the density of states near the Fermi level and on the low-frequency response functions.

Section II C presents the three-component optical conductivity of the high- T_c cuprates as a function of the static and elastic Raman vertices, with the relaxation processes taken into account in a phenomenological way. The present theory naturally introduces the concepts such as the effective number of conducting electrons and the high-frequency ($\hbar\omega > \hbar/\tau$) polarizability contributions which are strongly interrelated, instead of the quantities present in the usual two-component optical models (for example, the “free” and “bound” charge carriers). Additionally, the theory connects a small effective number of conducting electrons at $\delta \rightarrow 0$ with the “large” Fermi surface observed in the ARPES

measurements[18, 19].

Section III A discusses the conductivity sum rules of the three-band model. Several auxiliary frequencies are defined and compared with the frequencies of longitudinal collective modes. It is argued that the uncertainties in the present estimations of the model parameters originate mainly from a large inaccuracy in the experimental determination of the effective cut-off energies in the interband optical processes.

Section III B illustrates that the measured data in $\text{La}_{2-x}\text{Sr}_x\text{CuO}_4$, $0.1 < x < 0.2$, can be fitted reasonably by our seven-parameter optical model with the parameters nearly independent of doping. Measurements of the $x < 0.1$ compounds, on the other hand, reveal strong evidence on the large renormalization effects, requiring, at least, two different copper-oxygen bond energies. This issue, together with the abovementioned anomalies, is briefly discussed in Sec. III C within the ten-parameter version of the present model.

Although the resonant phenomena in the Raman-scattering experiments can be roughly explained by combining the present form of the elastic Raman vertices with the standard Raman correlation functions, the pronounced renormalization effects estimated here suggest a separate investigation of the Raman spectra.

II. THEORETICAL MODEL

A. Model A

The uncorrelated electrons described by the simplest version of the three-band model in the presence of the external vector potential polarized parallel to the conducting CuO_2 planes represent the optical model A. The complete Hamiltonian, shown in the hole picture, reads as

$$H = \sum_{L\mathbf{k}\sigma} E_L(\mathbf{k}) L_{\mathbf{k}\sigma}^\dagger L_{\mathbf{k}\sigma} - \frac{1}{c} \sum_{LL'\mathbf{k}\sigma} [A_\alpha(\mathbf{q}_\perp) J_\alpha^{LL'}(\mathbf{k}) \\ \times L_{\mathbf{k}+\mathbf{q}_\perp\sigma}^\dagger L_{\mathbf{k}\sigma}' + \text{H.c.}] + \frac{e^2}{2mc^2} \sum_{\mathbf{k}\sigma} [A_\alpha^2(\mathbf{q}_\perp) \\ \times (-)\gamma_{\alpha\alpha}(\mathbf{k}; 2) D_{\mathbf{k}+\mathbf{q}_\perp\sigma}^\dagger D_{\mathbf{k}\sigma} + \text{H.c.}]. \quad (1)$$

The bonding band ($L = D$) is partially occupied, and the antibonding and nonbonding bands ($L = P$ and N) are empty. Their dispersions are functions of the splitting between the oxygen and copper site energies, Δ_{pd} , and the first-neighbor bond energy, t_{pd} , and have the well-known form [for example, see Eqs. (A1) in Ref. 6]. $A_\alpha(\mathbf{q}_\perp)$ and $A_\alpha^2(\mathbf{q}_\perp)$ are the Fourier transforms in space of the vector potential $A_\alpha(\mathbf{r})$ and of its square $A_\alpha^2(\mathbf{r})$, respectively, and $\mathbf{q}_\perp \cdot \mathbf{a}_\alpha = 0$. $J_\alpha^{LL'}(\mathbf{k})$ are the current vertices, and $\gamma_{\alpha\alpha}(\mathbf{k}; 2)$ is the bare Raman vertex. The explicit form of these vertices is given in the Appendix A.

In the gauge invariant treatment of the optical conductivity (see Appendix C), the static and elastic Raman

vertices are of the central importance. As shown in the Appendix B, the former vertex is given by

$$\gamma_{\alpha\alpha}^0(\mathbf{k}) = \gamma_{\alpha\alpha}(\mathbf{k}; 2) + \frac{m}{e^2} \sum_{L=P,N} \frac{2|J_\alpha^{LD}(\mathbf{k})|^2}{E_{LD}(\mathbf{k})}, \quad (2)$$

and the latter one by

$$\gamma_{\alpha\alpha}^0(\mathbf{k}, \omega, \eta) = \gamma_{\alpha\alpha}^0(\mathbf{k}) - \frac{m}{e^2} \sum_{L=P,N} |J_\alpha^{LD}(\mathbf{k})|^2 \frac{(\hbar\omega)^2}{E_{LD}^2(\mathbf{k})} \\ \times \frac{2E_{LD}(\mathbf{k})}{(\hbar\omega + i\eta)^2 - E_{LD}^2(\mathbf{k})}, \quad (3)$$

with the abbreviation $E_{LL'}(\mathbf{k}) = E_L(\mathbf{k}) - E_{L'}(\mathbf{k})$. Notice that the elastic Raman vertex has an additional factor $(\hbar\omega)^2/E_{LD}^2(\mathbf{k})$ with respect to its usual form[7, 13, 20, 21]. This factor is a consequence of the gauge-invariance requirement[22].

B. Model B

The model B is a simple improvement of the model A. The influence of the charge-density fluctuations on the low-frequency (< 1.5 eV) optical conductivity is described here in the adiabatic approximation, by an effective (short-range) potential modulated with the wave vector $\mathbf{Q} = (\pi/a, \pi/a)$

$$H_{sr} = \sum_{\mathbf{k}\sigma} [J_{sr} D_{\mathbf{k}\sigma}^\dagger D_{\mathbf{k}+s\mathbf{Q}\sigma} + \text{H.c.}] \quad (4)$$

The sign s is chosen so that both vectors, \mathbf{k} and $\mathbf{k} + s\mathbf{Q}$, belong to the first Brillouin zone. The energy J_{sr} is assumed to be real, positive, independent of \mathbf{k} , and small in comparison with t_{pd} and Δ_{pd} . The treatment of the spin-density fluctuations, described by the spin-flip version of H_{sr} (where the typical contribution is of the form $J_{sr} D_{\mathbf{k}\uparrow}^\dagger D_{\mathbf{k}+s\mathbf{Q}\downarrow}$), leads to the same structure of the optical conductivity, and will not be considered as a separate case.

In the present approach, the emphasis is not on the energy dissipated in the electron scattering by the fluctuation fields (as usual for the $\mathbf{q} \approx 0$ external fields) but is instead on the large momentum dissipation. The (quasi)static treatment of the electron self-energy contributions originating from the (presumably antiferromagnetic) fluctuation fields is acceptable in the high- T_c cuprates in the range of dopings in which the energy scale associated with these fluctuations is small in comparison with the mid-infrared threshold energy (here equal to the difference between the Fermi energy and the van Hove energy). The major benefit of such radical simplification is the possibility to derive explicit analytical form for all topics relevant to the transverse optical theory, to verify the basic optical relations, and, finally, to compare the model predictions with the experimental data in detail.

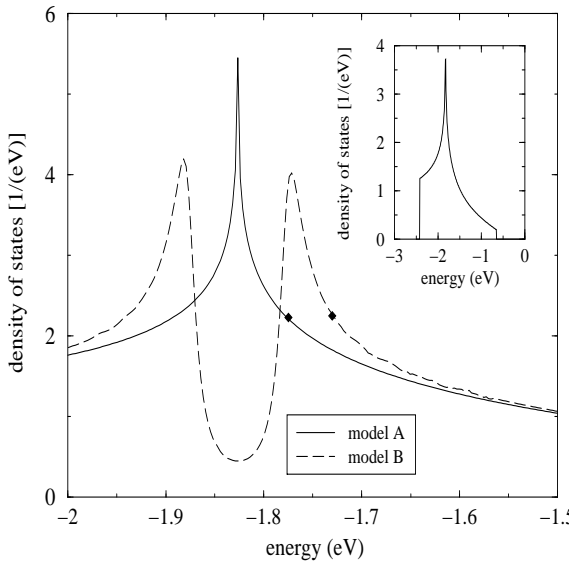


FIG. 1: Inset: The bonding-band density of states, $V_{pc}n_D(E)$, in the model A in the hole picture (V_{pc} is the primitive cell volume). Main figure: The effect of the perturbation (4) on $V_{pc}n_D(E)$ for $\eta = 10$ meV and $J_{sr} = 50$ meV, with $\Delta_{pd} \approx 0.66$ eV, $t_{pd} \approx 0.73$ eV, and $E_p = 0$. The density of states at the Fermi level for the doping $\delta = 0.2$ is represented by diamonds.

The perturbation (4) leads to the dimerization of the bonding band, resulting in the dispersions of the upper ($L = A$) and lower ($L = S$) subbands of the form

$$E_{A,S}(\mathbf{k}) = \frac{1}{2}[E_D(\mathbf{k}) + E_D(\mathbf{k} + s\mathbf{Q})] \pm \sqrt{\frac{1}{4}\varepsilon_{AS}^2(\mathbf{k}) + J_{sr}^2}, \quad (5)$$

with

$$\varepsilon_{AS}(\mathbf{k}) = E_D(\mathbf{k}) - E_D(\mathbf{k} + s\mathbf{Q}). \quad (6)$$

For simplicity, we restrict the analysis of the model B on the hole doped regime, $0 < \delta < 1$. In this case, the lower subband is fully occupied.

Fig. 1 illustrates the influence of the (quasi)dimerization on the density of states, calculated by replacing the δ function by a Lorentzian of half-width $\eta = 10$ meV:

$$n_D(E) = \sum_{L=S,A} \frac{1}{V} \sum_{\mathbf{k}^* \sigma} \frac{\eta/\pi}{[E_L(\mathbf{k}) - E]^2 + \eta^2}, \quad (7)$$

with the sum $\sum_{\mathbf{k}^*}$ restricted to the first Brillouin zone of the dimerized lattice ($\eta = 10$ meV corresponds roughly to $T \approx 100$ K). In contrast to the splitting of van Hove points by the intracell pp dimerization potential, which is relevant to the LTO/LTT phase transitions in $\text{La}_{2-x}\text{Ba}_x\text{CuO}_4$ [24], in the present case the pseudo-gap

structure in the density of states is associated with the intercell processes.

The effect of the (quasi)dimerization on the intraband optical conductivity can be described by the Raman vertices

$$\begin{aligned} \gamma_{\alpha\alpha}^{AA}(\mathbf{k}) &= \gamma_{\alpha\alpha}^0(\mathbf{k}) \cos \varphi_{\mathbf{k}} + \frac{m}{e^2} \frac{2|J_{\alpha}^{AS}(\mathbf{k})|^2}{E_{AS}(\mathbf{k})}, \\ \gamma_{\alpha\alpha}^{AA}(\mathbf{k}, \omega, \eta) &= \gamma_{\alpha\alpha}^{AA}(\mathbf{k}) - \frac{m}{e^2} |J_{\alpha}^{AS}(\mathbf{k})|^2 \frac{(\hbar\omega)^2}{E_{AS}^2(\mathbf{k})} \\ &\quad \times \frac{2E_{AS}(\mathbf{k})}{(\hbar\omega + i\eta)^2 - E_{AS}^2(\mathbf{k})}, \end{aligned} \quad (8)$$

with

$$J_{\alpha}^{AS}(\mathbf{k}) = J_{\alpha}^{DD}(\mathbf{k}) \sin \varphi_{\mathbf{k}}. \quad (9)$$

The auxiliary phase $\varphi_{\mathbf{k}}$ is given by

$$\cos \varphi_{\mathbf{k}} = \frac{\varepsilon_{AS}(\mathbf{k})}{E_{AS}(\mathbf{k})}, \quad \sin \varphi_{\mathbf{k}} = \frac{2J_{sr}}{E_{AS}(\mathbf{k})}. \quad (10)$$

We continue with the analysis of the optical conductivity by treating both of these two models in parallel. Since for $J_{sr} \ll \Delta_{pd}, t_{pd}$ the interband conductivity is not strongly influenced by the (quasi)dimerization, we shall approximate this contribution in the model B with that of the model A. Consequently, the difference between these two optical models will occur only in the intraband channel(s). Possible improvements in the description of the interband processes will be briefly examined at the end of the article.

C. Optical conductivity

According to the experimental observations and the discussion done in the Appendix C, the total optical conductivity of the high- T_c cuprates reads as

$$\begin{aligned} \sigma_{\alpha}^{\text{total}}(\omega) &\approx \frac{i}{\omega} \frac{e^2 n_c^{\text{eff}}}{m} \frac{\hbar\omega}{\hbar\omega + i\Sigma_1} - i\omega\alpha_{\alpha}^{\text{ir}}(\omega) \\ &\quad - i\omega\alpha_{\alpha}^{\text{inter}}(\omega) - \frac{i\omega}{4\pi} [\varepsilon_{\alpha,\infty}(\omega) - 1]. \end{aligned} \quad (11)$$

The four quantities which enter into this expression represent the effective number of conducting electrons per unit volume, n_c^{eff} , the mid-infrared polarizability, $\alpha_{\alpha}^{\text{ir}}(\omega)$, the interband polarizability, $\alpha_{\alpha}^{\text{inter}}(\omega)$, and the contribution of all other high-frequency optical processes, $\varepsilon_{\alpha,\infty}(\omega)$.

In similar multi-component optical models[3, 4, 8], concentrated primarily on the underdoped high- T_c cuprates, the first contribution is related to the “free” charge carriers and all other to the “bound” charge carriers, leading to the multi-oscillator form of the optical conductivity (usually, to the two-component low-frequency part) with a large number of adjustable parameters. On

the contrary, the measured low-frequency optical conductivities of the overdoped compounds[1, 2] support single-component models with strong quasiparticle damping effects. In spite of the simple treatment of the relaxation processes, the present optical model B is general. As will become clear below, it can explain both the single-component and two-component low-frequency conductivities. More importantly, the present model also allows a systematic study of the resonant effects observed both in the optical and Raman-scattering experiments[2].

In the model B, the first three terms are strongly interrelated. They depend only on the band parameters, which could be obtained from various other probes[27], and on three phenomenological damping energies Σ_i , representing the disorder effects. The straightforward calculation gives

$$n_c^{\text{eff}} = \frac{1}{V} \sum_{\mathbf{k}^* \sigma} \gamma_{xx}^{AA}(\mathbf{k}) [1 - f_A(\mathbf{k})], \quad (12)$$

$$\begin{aligned} \alpha_{\alpha}^{\text{ir}}(\omega, \Sigma_3) &= \frac{e^2}{m\omega^2} \frac{1}{V} \sum_{\mathbf{k}^* \sigma} [\gamma_{\alpha\alpha}^{AA}(\mathbf{k}, \omega, \Sigma_3) - \gamma_{\alpha\alpha}^{AA}(\mathbf{k})] \\ &\quad \times [f_A(\mathbf{k}) - 1], \\ \alpha_{\alpha}^{\text{inter}}(\omega, \Sigma_2) &\approx \frac{e^2}{m\omega^2} \frac{1}{V} \sum_{\mathbf{k}\sigma} [\gamma_{\alpha\alpha}^0(\mathbf{k}, \omega, \Sigma_2) - \gamma_{\alpha\alpha}^0(\mathbf{k})] \\ &\quad \times f_D(\mathbf{k}). \end{aligned} \quad (13)$$

The Fermi-Dirac function $[1 + e^{\beta[E_L(\mathbf{k}) - \mu]}]^{-1}$ is denoted by $f_L(\mathbf{k})$.

Since the contribution of the high-frequency processes is near zero below 3 eV, we take $\text{Im}\{\varepsilon_{\alpha,\infty}(\omega)\} = 0$ and $\text{Re}\{\varepsilon_{\alpha,\infty}(\omega)\} \approx \varepsilon_{\infty}$ in this energy region. For further considerations it is appropriate to denote the first three contributions to $\sigma_{\alpha}^{\text{total}}(\omega)$ by $\sigma_{\alpha}^{\text{Drude}}(\omega)$, $\sigma_{\alpha}^{\text{ir}}(\omega)$, and $\sigma_{\alpha}^{\text{inter}}(\omega)$, with the abbreviation $\sigma_{\alpha}^{\text{intra}}(\omega) \equiv \sigma_{\alpha}^{\text{Drude}}(\omega) + \sigma_{\alpha}^{\text{ir}}(\omega)$. Obviously, the optical conductivity of the model A follows on taking $J_{sr} = 0$, i.e., $\alpha_{\alpha}^{\text{ir}}(\omega) = 0$ and n_c^{eff} is given by Eq. (B3).

The corresponding macroscopic dielectric function reads as

$$\varepsilon_{\alpha}(\omega) = 1 + \frac{4\pi i}{\omega} \sigma_{\alpha}^{\text{total}}(\omega), \quad (14)$$

giving finally the optical model with seven adjustable parameters: t_{pd} , Δ_{pd} , J_{sr} , Σ_i , and ε_{∞} .

III. RESULTS AND DISCUSSION

As already mentioned in the Introduction, the main aim of the present paper is to establish the optical model that will make possible a reasonable fit of the measured real part of the optical conductivity of $\text{La}_{2-x}\text{Sr}_x\text{CuO}_4$, $0.1 < x < 0.2$, throughout the 0 to 3 eV region, as well as a fit of the corresponding real part of the dielectric function. In Sec. III A we introduce several useful topics related to the optical conductivity of the model B, and

then in Sec. III B we give *rough* estimates of seven adjustable parameters. At this point it should be recalled that, in order to fit *well* the optical conductivity in the high- T_c cuprates even in a small energy range, between 0 and 0.2 eV, one usually uses more than ten parameters.[3] To compare the present theory with such multi-oscillator approaches, we shall also show the improvements that occur in a naive generalization of the model B (Sec. III C).

A. General remarks

1. Conductivity sum rules

The total spectral weight of $\sigma_{\alpha}^{\text{total}}(\omega)$ can be represented, in principle, in two different ways. In the experimental analyses, it is natural to distinguish various contributions by using the spectral function $N_{\text{eff}}(\hbar\omega)$ defined by[1, 2]

$$N_{\text{eff}}(\hbar\omega) = \frac{8}{\Omega_0^2} \int_0^{\omega} d\omega' \text{Re}\{\sigma_{\alpha}^{\text{total}}(\omega')\}. \quad (15)$$

The frequency $\Omega_0 = \sqrt{4\pi e^2/(mV_{pc})}$, introduced here as the frequency-scale parameter, has in the La_2CuO_4 based compounds the value $\hbar\Omega_0 \approx 3.8$ eV.

Alternatively, several auxiliary frequencies, together with the associated effective numbers, can be defined by considering the spectral weight contained by the i -th channel [25]

$$\begin{aligned} \Omega_i^2 &= 4 \int_{-\infty}^{\infty} d\omega \text{Re}\{\sigma_{\alpha}^i(\omega)\}, \\ &\equiv V_{pc} n_i^{\text{eff}} \Omega_0^2. \end{aligned} \quad (16)$$

The index $i \in \{\text{total, intra, inter, Drude, ir}\}$. Notice that $n_{\text{Drude}}^{\text{eff}}$, defined by this relationship, is identical to n_c^{eff} , so that $\Omega_{\text{Drude}}^2 = V_{pc} n_c^{\text{eff}} \Omega_0^2$.

The conductivity sum rule of the three-band model is most appropriately described by

$$\Omega_{\text{total}}^2 = \Omega_{\text{Drude}}^2 + \Omega_{\text{ir}}^2 + \Omega_{\text{inter}}^2. \quad (17)$$

For the narrow bands with the relaxation processes negligible (limit $\Sigma_i \rightarrow 0$), the spectral function $N_{\text{eff}}(\hbar\omega)$ has a step-like form, with the steps simply related to Eq. (17). In the typical experimental situations, however, the relationship between these two representations is more complicated. Let us discuss now these issues at a more quantitative level.

In the model A, the total and intraband spectral weights are given in terms of the Raman vertices by

$$\begin{aligned} \Omega_{\text{total},0}^2 &= \Omega_0^2 \frac{1}{N} \sum_{\mathbf{k}\sigma} (-) \gamma_{\alpha\alpha}(\mathbf{k}; 2) f_D(\mathbf{k}), \\ \Omega_{\text{intra},0}^2 &= \Omega_0^2 \frac{1}{N} \sum_{\mathbf{k}\sigma} (-) \gamma_{\alpha\alpha}^0(\mathbf{k}) f_D(\mathbf{k}). \end{aligned} \quad (18)$$

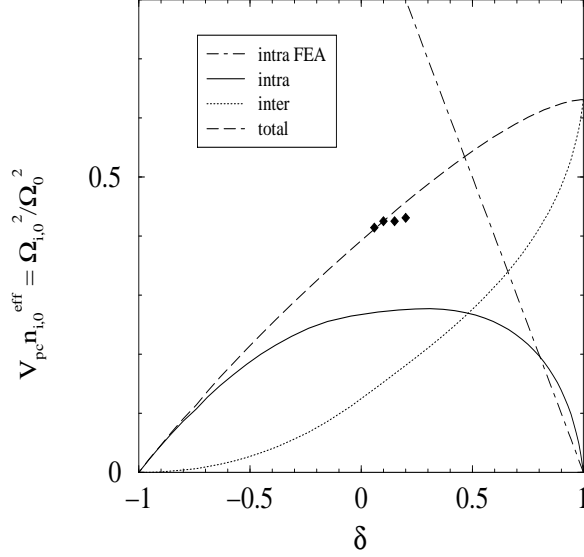


FIG. 2: The effective number of electrons in the model A as a function of δ ($\Delta_{pd} = 0.66$ eV, $t_{pd} = 0.73$ eV). Diamonds represent the values $N_{\text{eff}}(\hbar\omega_{\text{max}})$, $\hbar\omega_{\text{max}} = 3.0$ eV, measured in the $\text{La}_{2-x}\text{Sr}_x\text{CuO}_4$ compounds (Ref. 1) provided that $\delta = x$.

Similarly, they can be related to $N_{\text{eff}}(\hbar\omega)$ in the following way

$$\begin{aligned} \Omega_{\text{total},0}^2 &\approx N_{\text{eff}}(\hbar\omega_{\text{max}})\Omega_0^2, \\ \Omega_{\text{intra},0}^2 &\approx N_{\text{eff}}(\hbar\omega_{\text{min}})\Omega_0^2. \end{aligned} \quad (19)$$

$\hbar\omega_{\text{max}}$ and $\hbar\omega_{\text{min}}$ are, respectively, the effective maximal and minimal energy in the interband processes, which will be defined below.[26]

Fig. 2 illustrates the dependence of $\Omega_{\text{total},0}^2$ and $\Omega_{\text{intra},0}^2$ on the doping δ . For clarity, the prediction of the free-electron approximation (FEA) is also shown. It is important to notice that in the doping range $0 < \delta < 0.3$, which is relevant in the hole doped high- T_c superconductors, the total spectral weight is shared between the intraband and interband channels nearly in equal proportions. Furthermore, note that the derivative $\partial\Omega_{\text{inter},0}/\partial\delta$ is positive in this doping range, but small.

An appropriate description for the intracell charge distributions in the La_2CuO_4 based compounds has been established by the electric-field-gradient analysis, suggesting that $t_{pd}/\Delta_{pd} \approx 1.1$.[27] On the other hand, the bare interband absorption gap (that is, the charge-transfer gap) is near 1.75 eV. From these two informations, we obtain that the redistribution of spectral weight between the intraband and interband channels with increasing doping can be described by the parameters $t_{pd} = 0.73$ eV and $\Delta_{pd} = 0.66$ eV. Figures 2–10 present the results of the numerical calculations obtained in this way.

In the model B, developed on the assumption that $J_{sr} \ll t_{pd}, \Delta_{pd}$, we obtain

$$\Omega_{\text{total}}^2 \approx \Omega_{\text{total},0}^2,$$

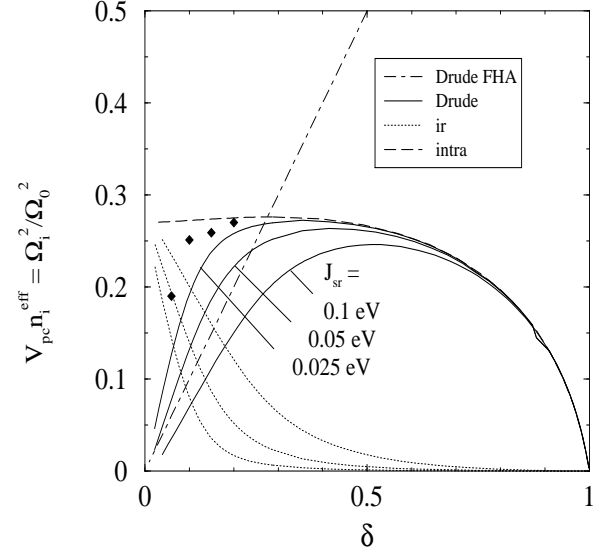


FIG. 3: The development of the intraband spectral weights with the perturbation J_{sr} , in the hole doped regime. The mid-infrared contribution is obtained by direct calculation, from Eq. (21), and the intraband and Drude contributions from the approximate expressions (20) and (22). The dot-dashed line is the prediction of the free-hole approximation (FHA). Diamonds represent the measured values $N_{\text{eff}}(\hbar\omega_{\text{min}})$ at $\hbar\omega_{\text{min}} = 2.0$ eV (Ref. 1).

$$\Omega_{\text{intra}}^2 \approx \Omega_{\text{intra},0}^2, \quad (20)$$

with the doping dependence already shown in Fig. 2. Furthermore, the spectral weight of the mid-infrared processes is given by

$$\begin{aligned} \Omega_{\text{ir}}^2 &= \Omega_0^2 \frac{1}{N} \sum_{\mathbf{k}^* \sigma} [\gamma_{\alpha\alpha}^{AA}(\mathbf{k}) - \gamma_{\alpha\alpha}^0(\mathbf{k}) \cos \varphi_{\mathbf{k}}] \\ &\times [f_A(\mathbf{k}) - 1], \end{aligned} \quad (21)$$

and that of the Drude term by

$$\Omega_{\text{Drude}}^2 \approx \Omega_{\text{intra},0}^2 - \Omega_{\text{ir}}^2. \quad (22)$$

The resulting spectral weights are illustrated for several values of J_{sr} in Fig. 3, exhibiting several interesting features.

First of all, it should be noted that the approximate expression for Ω_{intra}^2 , Eq. (20), is consistent with experiments throughout the 0.1 to 0.2 doping region provided that $\hbar\omega_{\text{min}} = 2.0$ eV. For $\delta < 0.1$, however, the discrepancy between these two values is significant, presumably reflecting the fact that the predicted values of the derivative $\partial\Omega_{\text{inter}}/\partial\delta$ are still positive.

Second, and more important, qualitative feature is the appearance of two different metallic behaviors: (i) the electronlike behavior characterized by $\partial\Omega_{\text{Drude}}/\partial\delta < 0$, and (ii) the holelike behavior where $\partial\Omega_{\text{Drude}}/\partial\delta > 0$. The critical doping δ_c , at which the behavior of the conducting electrons will be changed, depends on J_{sr} . For

$J_{sr} = 0.025$ eV, one obtains $\delta_c \approx 0, \pm 0.3$. In the present model, the holelike behavior at $\delta > 0$ is not primarily related to the presence of the second harmonic in the electron dispersion, as one usually assumes in the interpretation of the ARPES measurements, but is instead a consequence of the effective (quasi)dimerization potential.

Finally, notice that in the $0 < \delta < 0.1$ doping region the effective number of the conducting electrons obtained by the model (12) can be adequately described by the free-hole approximation. For example, the effective hole mass is $m^* \approx 0.5m$ for $J_{sr} = 0.025$ eV, or $m^* \approx 1.2m$ for $J_{sr} = 0.1$ eV.

2. Collective modes

The frequencies of the longitudinal collective modes are given by the zero crossings in the real part of the dielectric function. As easily seen from Eqs. (14) and (11), this function can be shown in the following form

$$\begin{aligned} \text{Re}\{\varepsilon_\alpha(\omega)\} = & \tilde{\varepsilon}_\infty - \frac{(\hbar\Omega_{\text{Drude}})^2}{(\hbar\omega)^2 + \Sigma_1^2} + 4\pi\text{Re}\{\alpha_\alpha^{\text{ir}}(\omega)\} \\ & + \alpha_\alpha^{\text{inter}}(\omega) - \alpha_\alpha^{\text{ir}}(\omega_0) - \alpha_\alpha^{\text{inter}}(\omega_0). \end{aligned} \quad (23)$$

Here $\tilde{\varepsilon}_\infty = \varepsilon_\infty + 4\pi\text{Re}\{\alpha_\alpha^{\text{ir}}(\omega_0) + \alpha_\alpha^{\text{inter}}(\omega_0)\}$ and ω_0 is a suitably chosen, auxiliary frequency (here $\hbar\omega_0 = 1.5$ eV; usually $\hbar\omega_0 \rightarrow \infty$). Before we compare the complete function $\text{Re}\{\varepsilon_\alpha(\omega)\}$ to the experimental data (Sec. III B), let us consider the zero crossings in some characteristic limits.

First, in the three-component model B with the relaxation processes negligible, three zero crossings are expected. The first one corresponds to the bare plasma energy, $\hbar\Omega_{\text{pl}}^0$. (In similar optical analyses this one is called the intraband plasma energy.[28]) The other two are placed in the vicinity of the bare mid-infrared and bare interband absorption gaps, $\Delta E_{\text{ir}} = E_A(\mathbf{k}_F) - E_S(\mathbf{k}_F)$ and $\Delta E_{\text{inter}} = E_N - E_D(\mathbf{k}_F)$.[29] (The latter energy is usually referred to as the interband plasma energy.)

In the single-band limit of the expression (23), in which the mid-infrared and interband polarizability contributions are disregarded, the plasma frequency is given by the well-known relation[6]

$$\hbar\Omega_{\text{pl}}^0 = \sqrt{(\hbar\Omega_{\text{Drude}})^2 / \tilde{\varepsilon}_\infty - \Sigma_1^2}. \quad (24)$$

The plasma frequencies measured in $\text{La}_{2-x}\text{Sr}_x\text{CuO}_4$ are shown in Fig. 4 and compared with the model predictions for $J_{sr} = 0$ and $J_{sr} = 0.1$ eV. Although this approximation gives correctly the holelike behavior at low hole doping, notice a large discrepancy between Ω_{pl}^0 and the measured frequencies.

Finally, for the damping energies quite large and δ not to small, the function $\text{Re}\{\varepsilon_\alpha(\omega)\}$ crosses zero again at

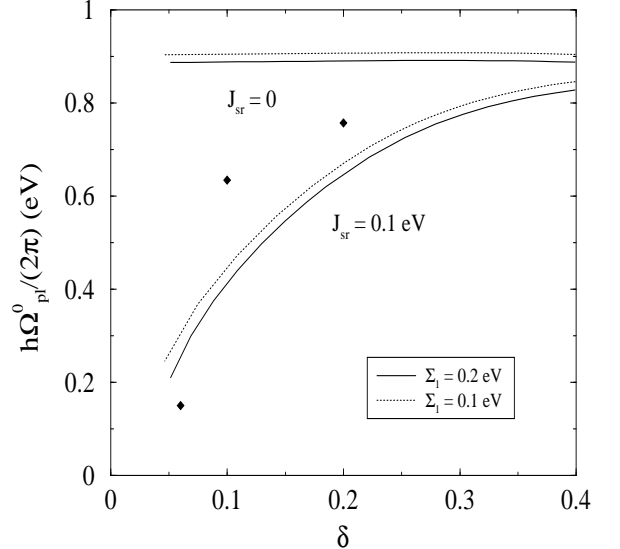


FIG. 4: The zero points of $\text{Re}\{\varepsilon_\alpha(\omega)\}$ as a function of the damping energy Σ_1 and the potential J_{sr} , according to the relation (24), with $\tilde{\varepsilon}_\infty = 4.7$. Diamonds represent the experimental data, Ref. 1.

one point, near Ω_{pl}^0 .[30] For large Σ_i but small doping level, where the number of conducting electrons is also small, the number of zero crossings as well as the shape of the function $\text{Re}\{\varepsilon_\alpha(\omega)\}$ become very sensitive on the value of Σ_3 . Compare Fig. 5, associated with the two-component low-frequency optical conductivity, to the real part of the dielectric function for $\delta = 0.2$ shown in Fig. 6, which characterizes an effective, nearly single-component low-frequency response.

3. Optical conductivity

The real part of the optical conductivity reads as

$$\begin{aligned} \text{Re}\{\sigma_\alpha^{\text{total}}(\omega)\} \approx & \frac{\hbar\Omega_{\text{Drude}}^2}{4\pi} \frac{\Sigma_1}{(\hbar\omega)^2 + \Sigma_1^2} \\ & + \omega \text{Im}\{\alpha_\alpha^{\text{ir}}(\omega, \Sigma_3) + \alpha_\alpha^{\text{inter}}(\omega, \Sigma_2)\}. \end{aligned} \quad (25)$$

When the polarizability contributions are disregarded, one obtains the counterpart of the expression (24), the Drude-like conductivity with the spectral weight Ω_{Drude}^2 . In contrast to the usual single-band models which require an additional parameter, the effective electron (hole) mass m^* , to explain the experimental spectral weights, in the present case Ω_{Drude}^2 is entirely determined by the parameters of the band model, and its value is controlled by the conductivity sum rule.

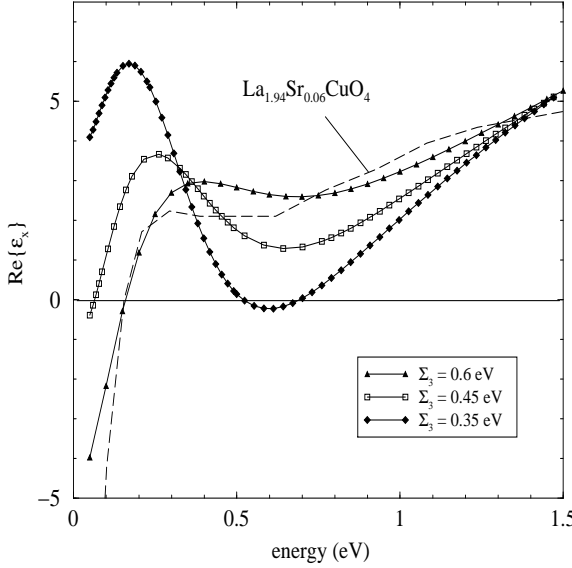


FIG. 5: The development of $\text{Re}\{\varepsilon_\alpha(\omega)\}$ with the damping energy Σ_3 , for $\delta = 0.06$, $\Sigma_1 = 0.2$ eV, $J_{sr} = 0.1$ eV, and $\tilde{\varepsilon}_\infty = 5.5$. The experimental data (Ref. 1) are represented by the long-dashed line.

B. $\text{La}_{1.8}\text{Sr}_{0.2}\text{CuO}_4$ compound – the complete fit in the model B

Starting from $\Delta_{pd} = 0.66$ eV and $t_{pd} = 0.73$ eV, we adjust the parameters J_{sr} , Σ_i , and $\tilde{\varepsilon}_\infty$ to obtain a reasonable fit of the dc conductivity and the spectral functions $\text{Re}\{\varepsilon_\alpha(\omega)\}$, $\text{Re}\{\sigma_\alpha^{\text{total}}(\omega)\}$, and $N_{\text{eff}}(\omega)$, measured at room temperatures (Ref. 1). As shown in Fig. 6, the discrepancy between the single-band expression for $\text{Re}\{\varepsilon_\alpha(\omega)\}$ (dotted line) and the experimental data can be remedied by taking the mid-infrared corrections into account. Notice that the required damping energy Σ_3 is huge in comparison with the energy J_{sr} , as well as in comparison with Σ_1 . The energy Σ_1 is huge itself when compared with the values found in the literature (typically, $\Sigma_1 = 50$ meV at room temperatures).

The low-frequency (< 1.5 eV) conductivity of all high- T_c cuprates is accompanied by a strong deviation from the simple Drude response. In the present model (see Fig. 7), the anomalous spectral weight in the energy range $\Sigma_1 < \hbar\omega < \Delta E_{\text{inter}}$ is comprised mainly of the infrared contributions and the subgap interband spectrum. A more accurate description for the fluctuation fields should give additional terms. One among them can be interpreted as resulting from the interplay between the bare interband and the bare mid-infrared processes. An additional broadening of both the mid-infrared and interband picks, arising from these residual processes, can be expected, resulting in a better agreement between the experiment and the theory than the one shown in Fig. 7. Interestingly, since the corresponding $\Omega_{\text{ir},0}^2 \approx 0$, the effect of such residual processes is negligible at $\delta \approx 0$.

The broadening of the interband pick will be strongly

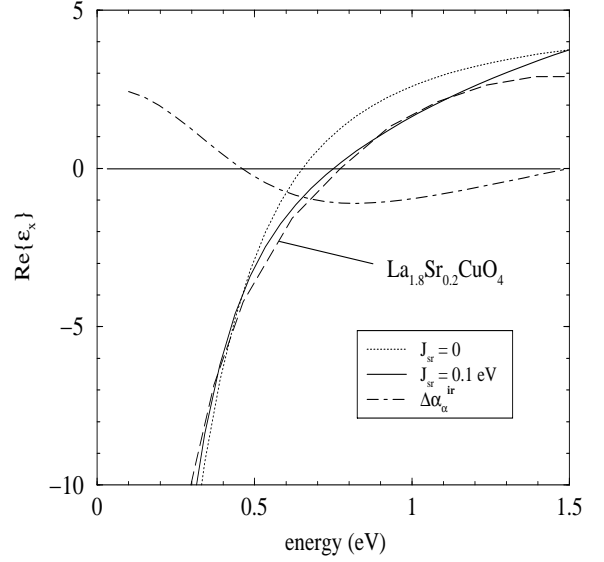


FIG. 6: The dependence of the real part of the dielectric function on J_{sr} for $\delta = 0.2$. Here $\alpha_\alpha^{\text{inter}}(\omega) - \alpha_\alpha^{\text{inter}}(\omega_0) = 0$, $\Delta\alpha_\alpha^{\text{ir}} \equiv 4\pi[\alpha_\alpha^{\text{ir}}(\omega) - \alpha_\alpha^{\text{ir}}(\omega_0)]$, $\Sigma_1 = 0.2$ eV, $\Sigma_3 = 0.5$ eV, and $\tilde{\varepsilon}_\infty = 4.7$.

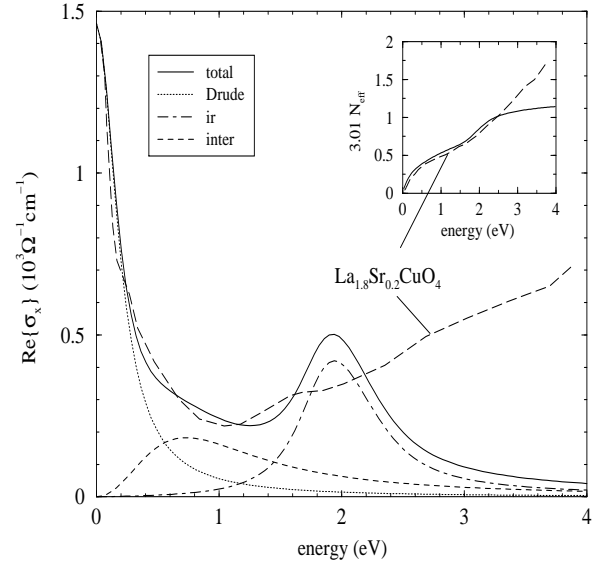


FIG. 7: The real part of the optical conductivity for $\delta = 0.2$, $\Sigma_1 = 0.2$ eV, $\Sigma_2 = 0.3$ eV, $\Sigma_3 = 0.5$ eV, and $J_{sr} = 0.1$ eV (solid line), compared with the room-temperature experimental data (long-dashed line). The contributions $\text{Re}\{\sigma_\alpha^i(\omega)\}$, $i \in \{\text{Drude, ir, inter}\}$, are also shown. Inset: The corresponding integrated spectral weight (in units of 10^3 eV $\Omega^{-1}\text{cm}^{-1}$).

enhanced by regarding in the bare Hamiltonian the band parameters which lift the degeneracy of the nonbonding band (in the first place, the oxygen-oxygen bond energy t_{pp}). However, this question requires a systematic study. Evidently, both of these effects are expected to lower the values of the damping energies Σ_2 and Σ_3 estimated here.

Let us turn back to Eqs. (19). The energy $\hbar\omega_{\min} \approx 2$ eV in Fig. 3 is chosen so that the spectral weight of the intraband contributions at $\hbar\omega > \hbar\omega_{\min}$ and that of the interband contributions at $\hbar\omega < \hbar\omega_{\min}$ are nearly equal to each other. The energy $\hbar\omega_{\max} \approx 3$ eV is obtained in the same way, by comparing the low-frequency and high-frequency contributions. Thus, the bare high-frequency absorption gap is near 3 eV. This conclusion is supported by similarity between the experimental and predicted integrated spectral weight,

$$\hbar \int_0^\omega d\omega' \operatorname{Re}\{\sigma_\alpha^{\text{total}}(\omega')\} \approx 3.01 N_{\text{eff}}(\hbar\omega) \times 10^3 \text{ eV } \Omega^{-1} \text{ cm}^{-1}, \quad (26)$$

shown on the inset of the figure.

In conclusion, the only way to fit all spectral functions in the considered energy range by the three-component model B with seven adjustable parameters is to use relatively large damping energies. Alternatively, one can disregard the conductivity sum rules and apply one of the multi-oscillator models[3], or the suitably modified model B, on a narrow energy scale. The fit with the modified ten-parameter model B is the subject of the next subsection.

C. Narrow-energy-scale fit in the modified model B

In order to perform a narrow-energy-scale analysis, it is convenient to introduce three additional adjustable parameters, by distinguishing external and internal single-particle potentials on the diagrams representing the i -th contribution to the total conductivity. They will be denoted by ζ_1 , ζ_2 , and ζ_3 , for the Drude, interband, and mid-infrared channel, respectively, with the corresponding spectral weights of the form

$$\Omega_i^2 \approx \zeta_i \Omega_{i,0}^2. \quad (27)$$

The values $\zeta_i \neq 1$, when combined with the sum rule (17), point at substantial missing spectral weights. We compare now the main effects caused by $\zeta_i \neq 1$ with the typical experimental results in the La_2CuO_4 based compounds. The missing spectral weights will not be considered. For simplicity, we consider only the case $J_{sr} = 0.1$ eV.

As already argued, two-component models do not fit well the low-frequency conductivity of $\text{La}_2\text{CuO}_{4+x}$.[3] Nevertheless, we can disregard the sum-rule requirement $\Omega_{\text{intra}}^2 = \Omega_{\text{Drude}}^2 + \Omega_{\text{ir}}^2$, and in this case we obtain a good fit of the Drude term (see Fig. 8). The energy $\Sigma_1 = 35$ meV is in agreement with earlier estimates[3, 4, 9]. Fig. 8 also illustrates that the original model B (i.e., the $\zeta_1 = 1$ case) overestimates significantly this low-frequency fraction of the spectral weight, but, as discussed above, fits reasonably Ω_{intra}^2 .

Fig. 9 displays in greater detail the evolution of the mid-infrared conductivity with Σ_3 . Again, it should be

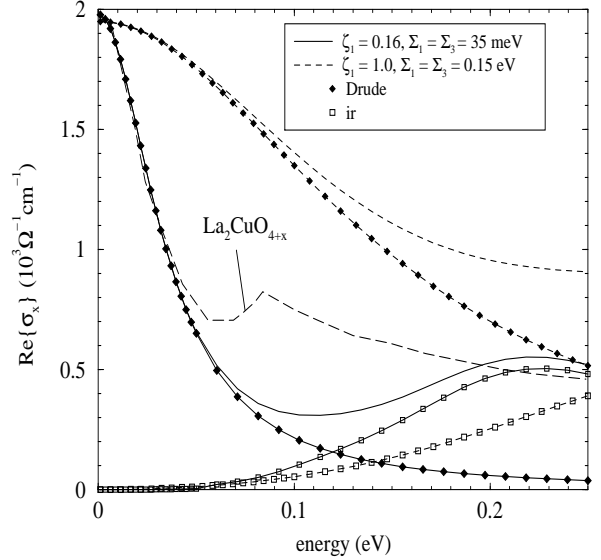


FIG. 8: The optical conductivity below 0.25 eV at various ζ_1 and Σ_3 for $\delta = 0.2$. The measured conductivity of $\text{La}_2\text{CuO}_{4+x}$ (long-dashed line) is from Ref. 3, $T = 200$ K.

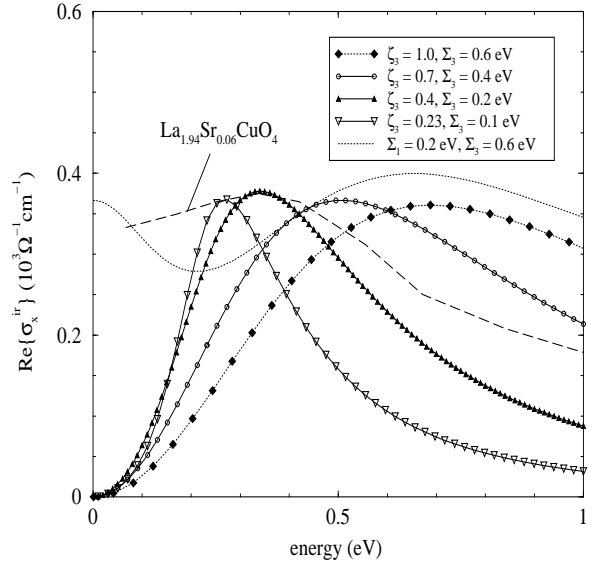


FIG. 9: The dependence of the mid-infrared contribution $\operatorname{Re}\{\sigma_\alpha^{\text{ir}}(\omega)\}$ on Σ_3 for $\delta = 0.06$. The dotted line represents the total conductivity for $\zeta_1 = 1$. The experimental data are from Ref. 1.

noted that the low-frequency (< 1.5 eV) spectrum transforms with decreasing doping from the nearly single-component structure at $\delta = 0.2$ (Fig. 7) into the two-component form at $\delta = 0.06$ (dotted line in Fig. 9).

This figure, together with Fig. 10, reveals the following generic feature of the polarizability contributions (see the related discussion of the gauge invariance in the Appendix C). In the underdamped (overdamped) regime, where the ratio between the damping energy Σ_i and the

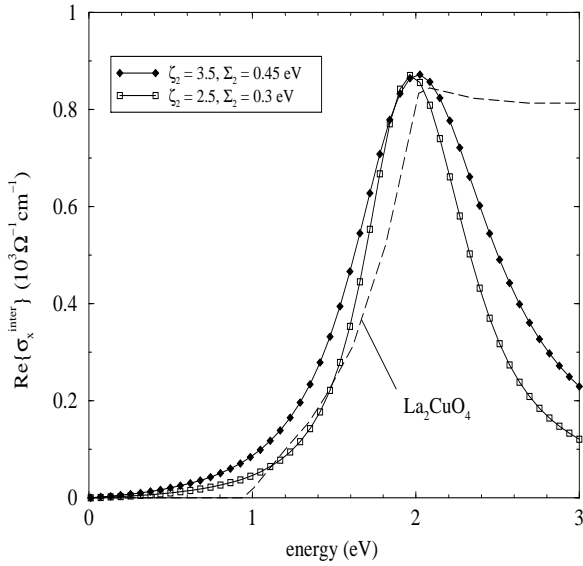


FIG. 10: The interband conductivity at various ζ_2 for $\delta \approx 0$. The experimental data are from Ref. 1.

absorption gap ΔE_i is small (large), the pick position in $\text{Re}\{\sigma_\alpha^i(\omega)\}$, $i \in \{\text{ir, inter}\}$, is controlled predominantly by the absorption gap ΔE_i (by the damping energy Σ_i). The anomalous hardening of the mid-infrared pick, when the doping decreases, can be thus associated with the increase in the damping energy Σ_3 , in the overdamped regime. On the contrary, Fig. 10 illustrates the dependence of the interband conductivity on Σ_2 in the underdamped regime. The increase in Σ_2 leads only to the broadening of the pick. Its position is not appreciably affected by Σ_2 .

The large and negative derivative $\partial\Omega_{\text{intra}}/\partial\delta$, observed for $x < 0.1$, is responsible for a systematic loss of the intraband conductivity with decreasing doping, and results in the complete disappearance of both the Drude and mid-infrared contributions at $x \approx 0$. Consequently, the solid lines on Fig. 10 also represent the total conductivity for $\delta \approx 0$, obtained within the eight-parameter model B. The optimal value of ζ_2 is given approximately by $\zeta_2 \approx \Omega_{\text{total},0}^2/\Omega_{\text{inter},0}^2$. According to Fig. 3, we obtain $\zeta_2 \approx 3$.

The discussion of Fig. 10 clearly demonstrates that the seven-parameter model B is inadequate to $\text{La}_{2-x}\text{Sr}_x\text{CuO}_4$, $0 < x < 0.1$. Instead, in this doping range, we can employ the eight-parameter model with ζ_2 estimated from $\zeta_2 \approx \Omega_{\text{inter,exp}}^2/\Omega_{\text{inter},0}^2$, and with $\zeta_1 = \zeta_3$ obtained on the basis of the conductivity sum rule. Not surprisingly, this naive generalization of the model B agrees with the slave-boson treatment of the Emery three-band model. The relationship $\zeta_2 \approx 1/b^2 \geq 1$ reflects the fact that the low-energy optical processes (associated with long time scales) have to be described by the renormalized band parameters and the interband ones (short time scales) by the bare band parameters (in the slave-boson approach, $t_{pd}^0 = t_{pd}/b$ and t_{pd} are,

respectively, the bare and renormalized bond energies, and b is the usual renormalization parameter). For $t_{pd}^0/\Delta_{pd}^0 = 1/3$ and $\delta \approx 0$ the slave-boson equations give $t_{pd}/\Delta_{pd} = 1.1$ and $b = 0.53$,[31] with $\zeta_2 \approx 3.5$.

IV. CONCLUSION

In this article, we have studied the influence of two dimerization potentials on the optical response of the conducting electrons in the high- T_c cuprates, and have compared the calculated spectral functions to that measured in $\text{La}_{2-x}\text{Sr}_x\text{CuO}_4$, $x < 0.2$. First, we consider the $0.1 < \delta < 0.2$ doping region, starting from the renormalized parameters of the optical model which are assumed to be independent of doping. It is found that the pd dimerization potential leads to the spectral weights of the intraband and interband channels nearly equal to each other. It is also shown that the (quasi)dimerization potential, introduced here to simulate the main effect of the short-range correlations on the low-frequency behavior of the conducting electrons, results in the non-Drude single-component intraband optical conductivity. Both of these results are in accordance with the experimental observations in the $0.1 < x < 0.2$ compounds. On the contrary, the calculated interband spectrum exhibits a pronounced pick, strongly contrasting the featureless measured spectrum.

In the framework of the present theory, the optical anomalies of the $x < 0.1$ compounds can be easily understood as a consequence of the reappearance of the bare band parameters in the high-frequency (> 1.5 eV) contributions to the response functions. The anomalous doping dependence of the intraband and interband spectral weights can be fitted by using an additional doping-dependent parameter (representing the ratio between the bare and renormalized copper-oxygen bond energies). It is argued that, due to the decrease in the effective number of conducting electrons, the intraband conductivity transforms naturally from a single-component into a two-component structure with decreasing doping. The anomalous hardening of the mid-infrared pick can be associated with the increase in the related disorder parameter. Interestingly, the discrepancy between the calculated and measured interband conductivities disappears with decreasing doping. The resulting description of the interband optical processes can be thus used as an appropriate starting point in the analysis of the resonant phenomena in the Raman-scattering experiments.

Acknowledgements

Useful discussions with Professor Slaven Barišić are gratefully acknowledged. This work was supported by Croatian Ministry of Science under the project 119-204.

APPENDIX A: VERTEX FUNCTIONS IN THE MODEL A

By using the auxiliary functions $u_{\mathbf{k}}$, $v_{\mathbf{k}}$, and $t_{\mathbf{k}}$, defined in Ref. 6, we obtain

$$J_{\alpha}^{DD}(\mathbf{k}) = \frac{e a t_{pd}^2}{\hbar} \frac{2u_{\mathbf{k}}v_{\mathbf{k}}}{t_{\mathbf{k}}} \sin \mathbf{k} \cdot \mathbf{a}_{\alpha}, \quad (\text{A1})$$

$$J_{\alpha}^{DP}(\mathbf{k}) = \frac{e a t_{pd}^2}{\hbar} \frac{u_{\mathbf{k}}^2 - v_{\mathbf{k}}^2}{t_{\mathbf{k}}} \sin \mathbf{k} \cdot \mathbf{a}_{\alpha},$$

$$J_x^{DN}(\mathbf{k}) = \frac{e a t_{pd}^2}{\hbar} \frac{2u_{\mathbf{k}}}{t_{\mathbf{k}}} \sin \frac{1}{2} \mathbf{k} \cdot \mathbf{a}_2 \cos \frac{1}{2} \mathbf{k} \cdot \mathbf{a}_1,$$

$$J_y^{DN}(\mathbf{k}) = -\frac{e a t_{pd}^2}{\hbar} \frac{2u_{\mathbf{k}}}{t_{\mathbf{k}}} \sin \frac{1}{2} \mathbf{k} \cdot \mathbf{a}_1 \cos \frac{1}{2} \mathbf{k} \cdot \mathbf{a}_2, \quad (\text{A2})$$

and

$$\gamma_{\alpha\alpha}(\mathbf{k}; 2) = \frac{m}{m_{xx}} \frac{\Delta_{pd} u_{\mathbf{k}} v_{\mathbf{k}}}{t_{\mathbf{k}}} \sin^2 \frac{1}{2} \mathbf{k} \cdot \mathbf{a}_{\alpha}. \quad (\text{A3})$$

The mass scale has the usual form $m_{xx} = \hbar^2 \Delta_{pd} / (2a^2 t_{pd}^2)$.

APPENDIX B: EFFECTIVE MASS THEOREM AND RELATED TOPICS

By comparing the static limit of the longitudinal and transverse response of the model A, we can verify several basic relations. First, the effective mass theorem connects two expressions for the dimensionless static Raman tensor

$$\begin{aligned} \gamma_{\alpha\alpha}^0(\mathbf{k}) &= (-) \frac{m}{\hbar^2} \frac{\partial^2 E_D(\mathbf{k})}{\partial k_{\alpha}^2} \\ &= \gamma_{\alpha\alpha}(\mathbf{k}; 2) + \frac{m}{e^2} \sum_{L=P,N} \frac{2|J_{\alpha}^{LD}(\mathbf{k})|^2}{E_{LD}(\mathbf{k})}. \end{aligned} \quad (\text{B1})$$

The related inverse \mathbf{k} -dependent effective mass reads as

$$(1/m) \gamma_{\alpha\alpha}^0(\mathbf{k}).$$

Secondly, the electron group velocity $v_{\alpha}^0(\mathbf{k})$ is given by

$$(-) v_{\alpha}^0(\mathbf{k}) = \frac{1}{\hbar} \frac{\partial E_D(\mathbf{k})}{\partial k_{\alpha}} = \frac{1}{e} J_{\alpha}^{DD}(\mathbf{k}). \quad (\text{B2})$$

Finally, the effective number of conducting electrons per unit cell $n_{c,0}^{\text{eff}}$ can also be shown in two equivalent forms (here $T \rightarrow 0$ K)

$$n_{c,0}^{\text{eff}} = \frac{1}{V} \sum_{\mathbf{k}\sigma} (-) \gamma_{\alpha\alpha}^0(\mathbf{k}) f_D(\mathbf{k}), \quad (\text{B3})$$

$$n_{c,0}^{\text{eff}} = m \frac{1}{V} \sum_{\mathbf{k}\sigma} |v_{\alpha}^0(\mathbf{k})|^2 \delta[E_D(\mathbf{k}) - \mu]. \quad (\text{B4})$$

The minus sign, $(-)$, in Eqs. (1) and (B1)–(B3) is a result of representing the electronlike dispersion $E_D(\mathbf{k})$

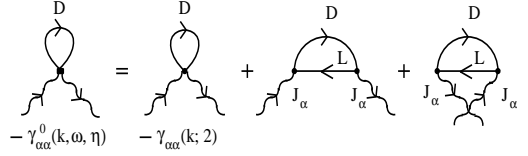


FIG. 11: The usual diagrammatic representation of the elastic Raman vertex, $L = N, P$. In the static limit, the summation gives the expression (B1), i.e. the inverse \mathbf{k} -dependent effective mass. The wavy and solid lines represent, respectively, the photon and electron Green functions.

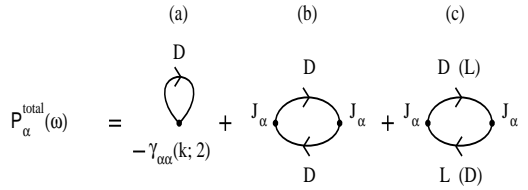


FIG. 12: The total photon self-energy in the model A, $L = N, P$.

in the hole picture. Notice that the form of $n_{c,0}^{\text{eff}}$ in the electron picture follows on taking that the fully occupied bonding band does not contribute to the dc conductivity, i.e. that $\sum_{\mathbf{k}} \gamma_{\alpha\alpha}^0(\mathbf{k}) = 0$. Consequently, in the electron picture one obtains[32]

$$n_{c,0}^{\text{eff}} = \frac{1}{V} \sum_{\mathbf{k}\sigma} \gamma_{\alpha\alpha}^0(\mathbf{k}) [1 - f_D(\mathbf{k})]. \quad (\text{B3}')$$

Beyond the static approximation, the effective second-order term in the electron-photon coupling comes from the contributions shown in Fig. 11. The elastic Raman vertex is the vertex function in such effective processes. The gauge invariant form of the elastic Raman vertex follows from the procedure explained in the Appendix C. The result is given by Eq. (3) in the main text.

APPENDIX C: OPTICAL CONDUCTIVITY OF THE MULTIBAND MODELS IN THE GAUGE INVARIANT TRANSVERSE APPROACH

The optical conductivity of the multiband models in which the dipolar transitions are absent can be obtained from the expression[33]

$$\frac{i\hbar}{\hbar\omega + i\eta_0} \frac{\Omega_0^2}{4\pi} \sum_i \mathcal{P}_{\alpha}^i(\omega, \eta_i). \quad (\text{C1})$$

Here $\mathcal{P}_{\alpha}^i(\omega, \eta_i)$ are the dimensionless photon self-energies, and η_i are the adiabatic terms (usually $\eta_0 = 0$).

Fig. 12 illustrates the diagrammatic representation of the photon self-energy contributions for the model A. The

diamagnetic self-energy, the Drude term, and the interband term [the diagrams (a)–(c) are given, respectively, by

$$\mathcal{P}_\alpha^{\text{total}} = V_{pc} n_{\text{total}}^{\text{eff}}, \quad (\text{C2})$$

$$\mathcal{P}_\alpha^{\text{Drude}}(\omega, \eta_1) = -\frac{i\eta_1}{\hbar\omega + i\eta_1} V_{pc} n_c^{\text{eff}}, \quad (\text{C3})$$

$$\begin{aligned} \mathcal{P}_\alpha^{\text{inter}}(\omega, \eta_2) &= \frac{m}{e^2 N} \sum_{\mathbf{k}\sigma} \sum_{L=N,P} |J_\alpha^{LD}(\mathbf{k})|^2 \\ &\times \left\{ \frac{f_D(\mathbf{k})}{\hbar\omega - E_{LD}(\mathbf{k}) + i\eta_2} \right. \\ &\left. - \frac{f_D(\mathbf{k})}{\hbar\omega + E_{LD}(\mathbf{k}) + i\eta_2} \right\}. \end{aligned} \quad (\text{C4})$$

Notice that the effective number n_c^{eff} in Eq. (C3) is equal to the expression (B4), representing the square of the electron group velocity averaged over the Fermi surface.

In the normal metallic state, the zero-frequency contribution to $\text{Re}\{\sigma_\alpha^{\text{total}}(\omega)\}$ has to vanish, even for $\eta_0 \neq 0$. This requirement leads to a basic optical relation

$$\sum_i \text{Re}\{\mathcal{P}_\alpha^i(0, \eta_i \approx 0)\} = 0 \quad (\text{C5})$$

[here $(0, \eta_i \approx 0)$ means the limit $\eta_i > \hbar|\omega|$, $\eta_i \rightarrow 0$]. Multiplied by Ω_0^2 , this relation gives the conductivity sum rule (17). Furthermore, rewritten in the form

$$\text{Re}\{\mathcal{P}_\alpha^{\text{total}} + \mathcal{P}_\alpha^{\text{inter}}(0, 0)\} = -\text{Re}\{\mathcal{P}_\alpha^{\text{Drude}}(0, \eta_1 \approx 0)\},$$

- [1] S. Uchida, T. Ido, H. Takagi, T. Arima, Y. Tokura, and S. Tajima, Phys. Rev. B **43**, 7942 (1991).
- [2] S. L. Cooper, D. Reznik, A. Kotz, M. A. Karlow, R. Liu, M. V. Klein, W. C. Lee, J. Giapintzakis, D. M. Ginsberg, B. W. Veal, and A. P. Paulikas, Phys. Rev. B **47**, 8233 (1993).
- [3] M. A. Quijada, D. B. Tanner, F. C. Chou, D. C. Johnston, and S.-W. Cheong, Phys. Rev. B **52**, 15 485 (1995).
- [4] S. Lupi, P. Calvani, M. Capizzi, and P. Roy, Phys. Rev. B **62**, 12 418 (2000).
- [5] G. Kotliar, P. A. Lee, and N. Read, Physica C **153–155**, 538 (1988); G. Kotliar, in *Correlated Electron Systems*, edited by V. J. Emery (World Scientific, Singapore, 1992), p. 118.
- [6] I. Kupčić, Phys. Rev. B **61**, 6994 (2000).
- [7] E. Ya. Sherman and C. Ambrosch-Draxl, Phys. Rev. B **62**, 9713 (2000).
- [8] V. J. Emery and S. A. Kivelson, Phys. Rev. Lett. **71**, 3701 (1993), V. J. Emery and S. A. Kivelson, Physica C **209**, 597 (1993).
- [9] T. P. Devereaux and A. P. Kampf, Phys. Rev. B **61**, 1490 (2000).
- [10] P. Prelovšek, A. Ramšak, and I. Sega, Phys. Rev. Lett. **81**, 3745 (1998).
- [11] G. Jackeli and N. M. Plakida, Phys. Rev. B **60**, 5266 (1999).
- [12] A. Zawadowski and M. Cardona, Phys. Rev. B **42**, 10

$$732 \quad (\text{C6})$$

it confirms the equivalence between the expressions (B3) and (B4).

To obtain the gauge invariant form of $\sigma_\alpha^{\text{total}}(\omega)$, we put $\eta_0 = 0$ and rearrange the expression (C1), so that

$$\sigma_\alpha^i(\omega) = \frac{i}{\omega} \frac{\Omega_0^2}{4\pi} [\mathcal{P}_\alpha^i(\omega, \eta_i) - \text{Re}\{\mathcal{P}_\alpha^i(0, \eta_i \approx 0)\}], \quad (\text{C7})$$

$i \in \{\text{Drude, inter}\}$. Next, these two expressions are rewritten in a compact form, and the adiabatic term in the numerator of $\sigma_\alpha^{\text{inter}}(\omega)$ is omitted. Finally, the disorder effects are taken into account in the phenomenological way, by $\eta_i \rightarrow \Sigma_i$. The result of this procedure is given by the two-component version of the expression (11). It is identical to the longitudinal optical conductivity [Eq. (50) in Ref. 6]. Notice that $\sigma_\alpha^{\text{inter}}(\omega)$, obtained in this way, has the structure similar to Eq. (C4), but the current vertices $J_\alpha^{LD}(\mathbf{k})$ are replaced by $(\hbar\omega/E_{LD})J_\alpha^{LD}(\mathbf{k})$.

The most important physical consequence of the above procedure is that in the metal-to-insulator phase transitions the dc conductivity disappears, at variance with the standard transverse approach [where $\sigma_\alpha^{\text{inter}}(\omega) \propto \mathcal{P}_\alpha^{\text{inter}}(\omega)$] in which the phenomenological treatment of the disorder leads to the non-physical results (for example, see the related discussion of the optical properties of the one-dimensional CDW insulators reported in Refs. 34, 35, 36).

- [13] T. P. Devereaux, Phys. Rev. B **45**, 12 965 (1992).
- [14] H. Nikšić, E. Tutiš, and S. Baršić, Physica C **241**, 247 (1995).
- [15] A. Sacuto, R. Combescot, N. Bontemps, C. A. Müller, V. Viallet, and D. Colson, Phys. Rev. B **58**, 11721 (1998).
- [16] M. Opel, R. Nemetschek, C. Hoffmann, R. Philipp, P. F. Müller, R. Hackl, I. Tütto, A. Erb, B. Revaz, E. Walker, H. Berger, and L. Forró, Phys. Rev. B **61**, 9752 (2000).
- [17] V. J. Emery, Phys. Rev. Lett. **58**, 2794 (1987).
- [18] R. Liu, B. W. Veal, A. P. Paulikas, J. W. Downey, P. J. Kostić, S. Fleshler, U. Welp, C. G. Olson, X. Wu, A. J. Arko, and J. J. Joyce, Phys. Rev. B **46**, 11 056 (1992).
- [19] A. Ino, C. Kim, T. Mizokawa, Z.-X. Shen, A. Fujimori, M. Takaba, K. Tamashaku, H. Eisaki, and S. Uchida, J. Phys. Soc. Jpn. **68**, 1496 (1999).
- [20] A. A. Abrikosov and V. M. Gorkov, Zh. Eksp. Teor. Fiz. **65**, 842 (1973) [Sov. Phys. JETP **38**, 417 (1974)].
- [21] N. W. Ashcroft and N. D. Mermin *Solid State Physics* (Saunders College Publishing, New York, 1976), Appendix E.
- [22] D. Pines and P. Nozières, *The Theory of Quantum Liquids I* (Addison-Wesley Publishing Co., Inc., New York, 1989), Chapter 4.
- [23] I. Kupčić (unpublished).
- [24] S. Baršić, Int. J. Mod. Phys. B **5**, 2439 (1991).
- [25] To simplify notation, we will refer to Ω_i^2 as the spectral

weight in the channel i . This differs from the usual normalization of the spectral weight by a factor 1/2.

[26] It has to be noted that the spectral functions $N_{\text{eff}}(\omega)$ measured in various layered cuprates confirm a large inaccuracy in the determination of $\hbar\omega_{\text{min}}$ and $\hbar\omega_{\text{max}}$. Nevertheless, the agreement between the experimental points and the model prediction on Figs. 2 and 3 can be adopted with one in ten accuracy.

[27] I. Kupčić, S. Barišić, and E. Tutiš, Phys. Rev. B **57**, 8590 (1998).

[28] P. Županović, A. Bjeliš, and S. Barišić, Z. Phys. B **101**, 387 (1996), and references therein.

[29] Obviously, there is a third threshold energy related with the optical transitions between the bonding and antibonding bands. However, for the model parameters considered here the coherence effects make the spectral weight of these processes negligible in comparison with the spectral weight of the $D \rightarrow N$ transitions, according to Ref. 6.

[30] Obviously, the multi-oscillator models with small oscillator widths and small oscillator strengths will also lead to one zero point.

[31] E. Tutiš, Ph. D. thesis, University of Zagreb, 1994.

[32] For free charge carriers, $\gamma_{\alpha\alpha}^0 = 1$, the expressions (B3) and (B3') lead, respectively, to $V_{pc}n_{c,0}^{\text{eff}} = 1 + \delta$ for free holes and $V_{pc}n_{c,0}^{\text{eff}} = 1 - \delta$ for free electrons.

[33] G. D. Mahan, *Many-particle Physics* (Plenum press, New York, 1990).

[34] L. Degiorgi, B. Alavi, G. Mihály, and G. Grüner, Phys. Rev. B 44, 7808 (1991).

[35] L. Degiorgi, St. Thieme, B. Alavi, G. Grüner, R. H. Mckenzie, K. Kim, and F. Levy, in *Physics and Chemistry of Low-Dimensional Inorganic Conductors*, edited by C. Schlenker et al., (Plenum press, New York, 1996), p. 337.

[36] K. Kim, R. H. Mckenzie, and J. W. Wilkins, Phys. Rev. Lett. 71, 4015 (1993).